Eur. Phys. J. D **12**, 185–192 (2000)

THE EUROPEAN PHYSICAL JOURNAL D

EDP Sciences

Charge transfer between alkali cluster ions and atoms in the 1 to 10 keV collisional energy range

C. Bréchignac, Ph. Cahuzac[a], B. Concina, J. Leygnier, and I. Tignères

Laboratoire Aimé Cotton, CNRS, Bâtiment 505, Campus d'Orsay, 91405 Orsay Cedex, France

Received 13 April 2000 and Received in final form 29 June 2000

Abstract. The cross-sections for collisional charge transfer between singly charged free clusters M_n^+ (M = Li, Na; $n = 1...50$) and atomic targets A (cesium, potassium) have been measured as a function of collisional relative velocity in laboratory energy range 1–10 keV. For each cluster size, the experimental values of the charge transfer cross-section $\sigma(v)$ are fitted with an universal parametric curve with two independent parameters σ_m and v_m, the maximum cross-section and the corresponding velocity. For small size clusters ($n \leq 15$), the $\sigma(v)$ characteristic parameters show strong variations with the number of atoms in the cluster. Abrupt dips observed for $n = 10$ and $n = 22$ are attributed to electronic properties. Charge transfer patterns observed for various collisional systems present similarities, which appear more sensitive to cluster quantum size effects than to collision energy defects. In their whole, the σ_m and v_m parameters show differences in both their size evolution and their absolute values discussed in term of projectile and target electronic structures.

PACS. 36.40.-c Atomic and molecular clusters – 36.40.Jn Reactivity of clusters – 36.40.Cg Electronic and magnetic properties of clusters – 34.70.+e Charge transfer

1 Introduction

Most of the information which has been obtained about electronic properties of metal clusters over the past years comes from the studies of cluster response to external electromagnetic fields. Static polarizabilities, giant dipole resonances, ionization potentials, and photoelectron spectra have been studied both experimentally and theoretically [1,2]. The results deal with interaction within a long time scale as compared to nuclei motions. More recently have been carried out new studies devoted to the metal cluster electronic response at a time scale for which nuclear motions are frozen, by using for example femtosecond laser [3,4] or keV collisions with atoms or protons [5–9] in order to disentangle electronic properties from nuclear motion. Collisions involving alkali clusters at laboratory energies between 1 and 10 keV correspond to the situation where nuclei can still be considered as fixed during the collision and where relative velocities of approach are small compared to the orbital velocity of external electron motion (adiabatic description) [7,8].

The direct observation of an electron transfer from an atom or a molecule to a small metallic particle is of primary interest in surface science and catalysis, since an electron jump is often the first step of a chemical reaction. A fundamental question is for which cluster size the colliding partner interacts either with the whole cluster or only with a part of it? from which cluster size does the interaction resemble an atom-surface interaction? Studies of the evolution of charge transfer properties between clusters and atoms as a function of particle size is a way to address these questions.

Experimental data already available on electron transfer concern either the possibility to form mass selected neutral clusters by collisional neutralization of mass selected cluster ions [10–13] or to estimate cluster ionization potentials [14]. In the first case, the reionization of the neutral products obtained for $Na_n^+ + Cs$ collisions shows that most of them do not undergo any fragmentation [5], suggesting that charge transfer is an efficient way to produce mass selected neutral species.

Measurements on Na_n^+ and K_n^+ charge transfer cross-sections with cesium atoms have been interpreted using the Rapp and Francis formalism [15]. No systematic studies with the collision energy have been carried out up to now.

In the present paper we present systematic measurements of charge transfer cross-section (C.T.) for $M_n^+ + A$ collisions. The projectiles M_n^+ are n-numbered lithium or sodium cluster ions ($1 < n < 50$), the target A is a cesium or a potassium atom. The collision energy in the laboratory frame varies from 1 keV to 10 keV. We describe in Section 2 the experimental arrangement and our methodology, and Section 3 presents the results and the discussion. For a given couple ($M_n^+ + A$), we focus on the evolution of the charge transfer efficiency with cluster velocity

[a] e-mail: philippe.cahuzac@lac.u-psud.fr

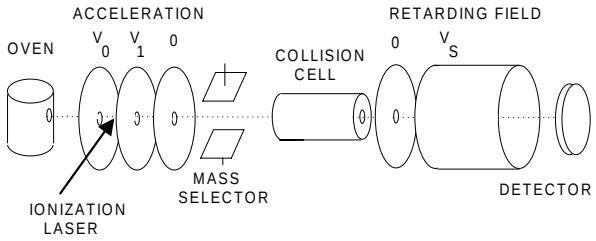

Fig. 1. Schematic diagram showing the basic elements of the apparatus. Mass dispersed cluster ions interact with target atoms. The detector collects either charged and neutral collision products when $V_s = 0$, or only neutral products when $V_s > V_0$.

and size, and compare the results obtained when changing the projectile and the target.

The main findings can be summarized as follows. The velocity dependence of charge transfer cross-section between a cluster ion and a neutral atom exhibits the typical features of a non-resonant atom-ion charge transfer cross-section profile. The maximum cross-section decreases as cluster size increases. The velocity at maximum decreases as cluster size increases, and qualitatively follows, for large sizes, the Massey criterion. Charge transfer involving small metallic particles partly reflects the cluster electronic properties.

2 Experimental procedure

2.1 Experimental arrangement

We carried out size-resolved measurements of integral collisional charge transfer cross-sections when a beam of accelerated cluster ions propagates through a heat-pipe-like cell [16] containing the target vapor (Cs or K). The pressure in the cell is determined by the temperature and kept low enough to insure single collision conditions.

A schematic diagram showing the main elements of the apparatus is given in Figure 1. Neutral alkali clusters are first produced in a gas aggregation source. Alkali vapor effuses into He gas (20 mbar pressure). Downstream from the oven, the nucleation takes place in a copper tube cooled with flowing liquid nitrogen. Metal clusters condense out of the quenched vapor and are carried out by the gas stream through two differential pumping chambers into a high vacuum chamber. They are then ionized and accelerated in the entrance region of a Wiley-Mc Laren [17] tandem time-of-flight mass spectrometer [18]. The ionizing photons are delivered by a Nd–YAG laser at an energy $h\nu = 3.50$ eV. The ionizing laser fluence is kept high enough to ionize, photoexcite and warm the clusters during the 15 ns pulse duration. Rapid sequential evaporation steps occur during the 1 μs residence time in the ionizing region resulting in an ion cluster distribution shifted down toward lower masses. Under these experimental conditions, each observed mass is produced by the evaporation of a larger one. This corresponds to an "evaporative ensemble" situation [19]. Metal clusters produced in those conditions contain an internal vibrational energy corresponding to a temperature in the range 500–700 K for lithium clusters [20] and 300–400 K for sodium clusters [22].

Cluster ions are accelerated to a final ion beam energy set between 1 and 10 keV before entering the first time-of-flight of the mass spectrometer where they resolve into individual mass packets. A mass dispersed singly charged cluster packet enters the heat-pipe-like cell through a 4 mm diameter diaphragm and collides with target atoms. The collision products propagate through the second time-of-flight spectrometer and reach a Micro Sphere Plate detector (El Mul) [21] of diameter 2.5 cm, larger than the cluster beam diameter. This drift region is field free in order to have the same trajectories for neutral and charged particles.

The detector front face is grounded in order to have similar collection efficiency for charged and neutral clusters. A system of grids and electrostatic shields allows us either to stop the ions or to disperse them using the retarding field method (potential V_s). Consequently, the experimental procedure is as follows. The collision cell temperature is stabilized at a target density n_A ranging from 5×10^9 up to 5×10^{12} at/cm^3. For a given ion beam kinetic energy eV_0, we measure the mass spectrum peak intensities with no retarding potential ($V_s = 0$). The n-mer mass peak contains the charged and neutral products due to the collision $M_n^+ + A$. By setting $V_s \geq V_0$, charged particles are stopped and the detected mass peaks contain only the neutral products. For a given parent cluster size, we measure the signal $S_i + S_n$ ($V_s = 0$) and S_n ($V_s \geq V_0$) to deduce the neutralization ratio $r_n(n_A) = S_n/(S_i + S_n)$. This operating mode allows a simultaneous measurement on the whole mass spectrum. It is fast enough to avoid problems with source fluctuations or slow target density variations during the whole measurements.

2.2 Charge transfer and collision induced dissociation

The procedure described above allows us to measure the signal of neutral particles produced from mass selected M_n^+ cluster parents, but these neutral fragments can arise from three different physical processes:

(a) Unimolecular Decay (U.D.),

(b) Collision Induced Dissociation (C.I.D.),

(c) cluster neutralization by Charge Transfer (C.T.).

Unimolecular Decay comes from the dissipation of the internal energy contained in a warm cluster parent during the time of flight. Collision Induced Dissociation corresponds to the evaporation of the cluster parent following an inelastic collision in the heat-pipe cell [15]. We have previously shown that alkali clusters evaporate monomers

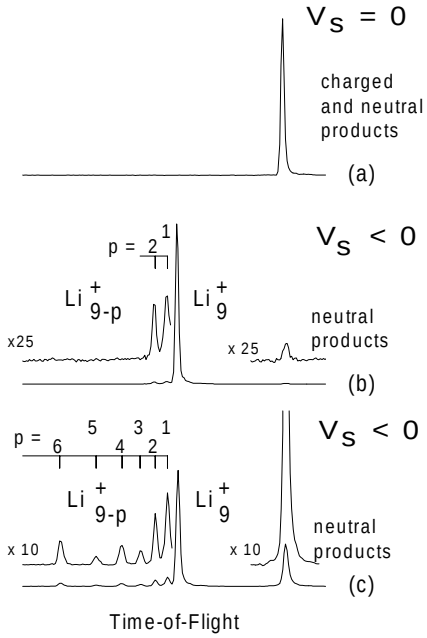

Fig. 2. Time-of-flight spectra obtained after Li_9^+ + Cs collisions, at a laboratory energy 5000 eV. Trace (a): no electrostatic dispersion, $V_s = 0$. Trace (b): $\sigma_{C.T.} n_A l \ll 1$, no collisions. The charged fragments coming from U.D. are mass dispersed ($V_s < 0$). Trace (c): single collision regime, and dispersion of the charged collision fragments ($V_s < 0$). The light charged fragments come from C.I.D. The neutral products peak contains mainly particles obtained by C.T. and very few neutral species due to U.D. and C.I.D.

or dimers [20,22]. The reactions are

$$\begin{array}{lll} & & M_{n-1}^+ + M \\ \text{U.D.} & M_n^+ & \nearrow \\ & & \searrow \\ & & M_{n-2}^+ + M_2 \\ \text{C.I.D.} & M_n^+ + A \longrightarrow & M_{n-q_1-2q_2}^+ + q_1 M + q_2 M_2 + A \\ \text{C.T.} & M_n^+ + A \longrightarrow & M_n + A^+. \end{array}$$

As illustrated in Figure 2 for Li_9^++Cs collision, we checked in separate experiments that the observed neutral particles come essentially from C.T. and not from U.D. or C.I.D. processes. Figure 2a is obtained when the stopping potential V_s is set to 0 and at a very low cesium density so that no C.T. takes place. The peak contains the mass selected Li_9^+ and the fragments due to unimolecular decay during the time-of-flight. These masses all have the same time of flight. Figure 2b is obtained with $V_s < 0$. Charged fragments are separated from neutral ones and mass analyzed, the lightest charged fragments reaching the detector earlier in time. The relative intensities of Li_8^+ and Li_7^+ peaks coming from Li_9^+ U.D. are less than 3% and the corresponding detected neutral fragment peak is even weaker. Figure 2c corresponds to the same mass dispersion analysis but at a cesium density 10^3 larger. From Figure 2b we evaluate the C.I.D. contribution to the neutral peak. It remains small compared to the contribution of charge transfer.

The peak containing the C.T. and C.I.D. neutral fragments is more intense. However, the C.I.D. charged fragment peaks are not much larger than those of U.D. so that the contribution of the C.I.D neutral products to the measured neutral peak is not significant. We note that for neutral particles having the same velocity, the detection efficiency is lower for the C.I.D. fragments which are composed of light particles (monomers or dimers) than for the C.T. products of heavier masses. The predominance of C.T. over C.I.D. has been verified for all the other parent clusters in the considered mass range.

We checked earlier [5] and under the same experimental conditions the two following points:

(a) the neutralization ratio r_n evolution with target density n_A corresponds to Beer's law $r_n(n_A) = r_n(0)(1 - \exp(-\sigma n_A l))$ where l is the collision cell length. We worked with neutralization ratio lower than 20%, in order to insure a single collision regime;
(b) most of the neutral clusters produced by collisional charge transfer do not fragment. This point has been demonstrated by reionization of the neutral charge transfer products which have been mass analyzed by time-of-flight mass spectrometry [5].

The neutral products have the same mass and velocity as the parent ions, insuring the same detection efficiency for both species. Because the detector collects all the products, we can compare quantitatively the charged and neutral cluster signals and the measured neutralization ratio is meaningful.

It has been shown for atomic or molecular systems that collisional charge transfer takes place at large impact parameters with near-zero momentum transfer [23]. We verified here in the mass spectra that the neutral and the corresponding ion mass peaks have the same time of flight profile. This indicates the absence of significant momentum transfer associated with the cluster ion-atom charge transfer collision. We also checked that for the target densities used here, the sum of ionic and neutral signal equates to the primitive ion signal obtained with a negligible target density. Consequently, C.T. measurements are not affected by scattering processes which could drive the particles out of the detector acceptance angle.

2.3 Calibration

A key point in the measurements of *absolute* cross-sections is the calibration. It is difficult to know accurately the atomic target density along the cell. In order to overcome this problem, we measured neutralization rates for M^+ + Cs ion-atom collisions and deduced the target cell density using the absolute cross-sections previously measured at the same velocity by Perel and Daley [24] ($\sigma = 38$ Å^2 for $Na^+ + Cs$ collision at relative velocity 1.8×10^5 m/s, $\sigma = 120$ Å^2 for $Li^+ + Cs$ collision at relative velocity 3.2×10^5 m/s and $\sigma = 50$ Å^2 for $Li^+ + K$ collision at relative velocity 3.2×10^5 m/s). With this calibration method, our $M^+ + A$ C.T. cross-sections profiles are in good agreement

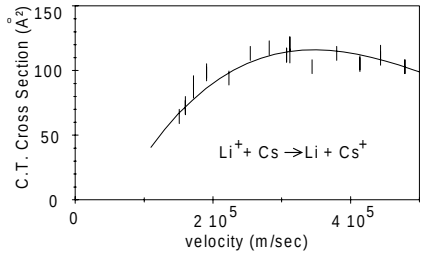

Fig. 3. $Li^+ + Cs$ collisional charge transfer: $\sigma(v)$ profile measured by Perel and Daley (full line), and results obtained during this work using the calibration $\sigma = 120$ Å^2 at 3.2×10^5 m/s.

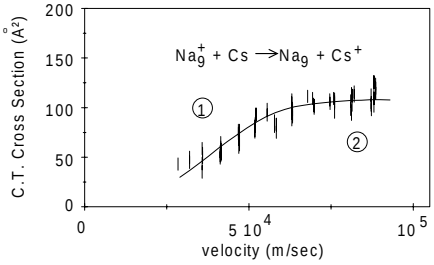

Fig. 4. Absolute charge transfer cross-section for $Na_9^+ + Cs$ collision plotted *versus* collision relative velocity. Error bars on cross-section points represent one standard deviation of the data.

with Perel and Daley data, for laboratory collision energies between 1 and 10 keV (Fig. 3).

3 Results and discussion

3.1 Charge transfer cross-section profiles

Charge transfer cross-sections for the collisions $M_n^+ + A \longrightarrow M_n + A^+$ are measured as a function of collision relative velocity. Figure 4 shows the absolute charge transfer cross-section profile for $Na_9^+ + Cs$ collision *versus* relative velocity (C.T. profiles). It reflects the typical features of non resonant C.T. collisions [25]. The cross-section is small at low velocity and increases rapidly with increasing velocity (velocity threshold, part 1). It levels off to a broad maximum (part 2) then it is expected to decrease.

The $Na_n^+ + Cs$ C.T. profiles can be compared to the calculations recently published by Knospe *et al.* (microscopic analysis using non adiabatic quantum molecular dynamics [9]). The measured C.T. velocity profiles behave qualitatively as the calculated ones, but the measured absolute values are larger by a factor of five. Moreover the velocity dependence is in agreement for $n = 9$ but is slightly shifted for $n = 4$ and $n = 7$.

In order to compare the C.T. cross-section measurements as a function of collision velocity for the various reactions $M_n^+ + A$, it is convenient to use a parametric curve for a fit of the experimental $\sigma(M_n^+ + A)$ cross-sections, as a guide line. For sake of simplicity we used the velocity profile calculated for ion-atom non resonant collisions, *i.e.*

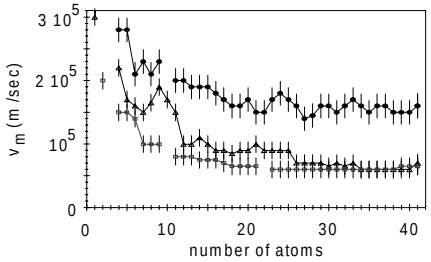

Fig. 5. Representation of the velocity corresponding to the maximum charge transfer cross-section (v_m), obtained by a fit of the data, as a function of the cluster atom number n for $Na_n^+ + Cs$ (□), $Li_n^+ + Cs$ (△) and $Li_n^+ + K$ (●) collisional systems.

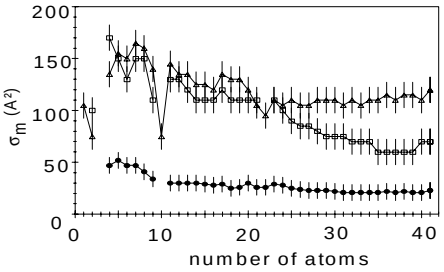

Fig. 6. Representation of the absolute C.T. cross-section at the maximum of the velocity profile (σ_m), as a function of cluster atom number n for $Na_n^+ + Cs$ (□), $Li_n^+ + Cs$ (△) and $Li_n^+ + K$ (●) collisional systems.

the reduced Olson profile [26] Q^*

$$\sigma(v) = \frac{\sigma_m}{1.08} Q^* \left(3.1 \frac{v}{v_m} \right). \quad (1)$$

The numerical factors 1.08 and 3.1 are such that the two independent parameters v_m and σ_m correspond respectively to the velocity and the amplitude for which the profile reaches the maximum [27]. We obtain a set of parameters which characterize the C.T. cross-section velocity profiles for various collisional partners. These parameters v_m and σ_m are plotted *versus* the projectile number of atoms n for the three collisional studied systems: $Na_n^+ + Cs$, $Li_n^+ + Cs$ and $Li_n^+ + K$ (Figs. 5 and 6).

Due to the limited range of cluster acceleration (1 to 10 keV), the measured C.T. cross-sections obtained for the three collisional systems lie in finite parts of the velocity curves: part 1 and part 2 for $Na_n^+ + Cs$ (see Fig. 4), end of part 1 and part 2 for $Li_n^+ + Cs$, part 1 and beginning of part 2 for $Li_n^+ + K$. Consequently, the parameters are determined within ±10% for $Na_n^+ + Cs$ collisions and ±15% for the other systems.

For small clusters ($n < 20$), superimposed on a general decrease as the size increases, σ_m and v_m parameters present sharp variations from one size to the next one. For larger cluster sizes, except for $\sigma_m(Na_n^+ + Cs)$ which still decreases with the size, the parameters approach nearly constant values which depend on the nature of the colliding partners.

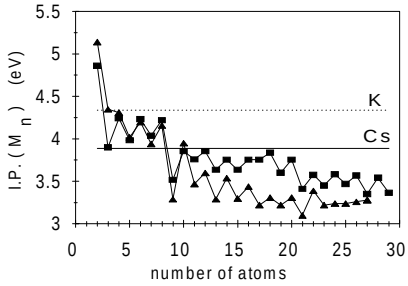

Fig. 7. Plot of ionization potential *versus* n for lithium (▲) and sodium clusters (■). The full and dashed lines are for I.P.(Cs) = 3.89 eV and I.P.(K) = 4.39 eV respectively.

3.2 Charge transfer cross-section profiles and target element

Electron transfer from the target A to the metal cluster M_n^+ depends on both the target and the projectile properties. The role played by the target is emphasized by comparing Li_n^+ + Cs and Li_n^+ + K charge transfer cross-sections. Changing the target implies modifications in the collisional energy defect and in the representation in terms of hard sphere or in the electronic cloud overlap of the collisional partners. We discuss these different approaches.

As a starting point the role of the collision energy defect can be discussed in the light of the Massey criterion. It allows a qualitative approach of non resonant collisions [28,29]. It expresses that at the maximum of the cross-section associated to the process, the typical interaction time duration $T_{\Delta E} = h/\Delta E$ equals the collision time duration τ. If ΔE is the total energy change [28,29], and a the typical interaction length, the velocity at the maximum cross-section is

$$v_m \simeq \frac{a}{h}|\Delta E|. \tag{2}$$

Assuming that the electron transfer involves only ground states of the partners, ΔE is the ionization potential (I.P.) difference

$$\Delta E = \text{I.P.}(\text{M}_n) - \text{I.P.}(\text{A}). \tag{3}$$

The interaction length is of the order of the Bohr radius in the case of atom-atom collisions. In Figure 7 are plotted the ionization potentials I.P.(M_n) and I.P.(A). The data are taken from literature for sodium clusters [1], lithium clusters [30] and for the alkali atoms [31]. It appears that when n increases, $|\Delta E|$ increases (at least beyond $n = 8$ with Cs as target) while v_m is found to decrease. This suggests a size dependence of a. Calculations show a decrease of the interaction length from $a = 25$ Å around $n = 8$ down to $a = 5$ Å at largest sizes. It is interesting to note that these values lie in the range in between typical values deduced from ion-atom charge transfer [29] and those usually considered for atom-surface interaction [32]. It is also remarkable that for the largest sizes ($n \geq 25$) the larger ΔE, the larger v_m, in agreement with the Massey criterion.

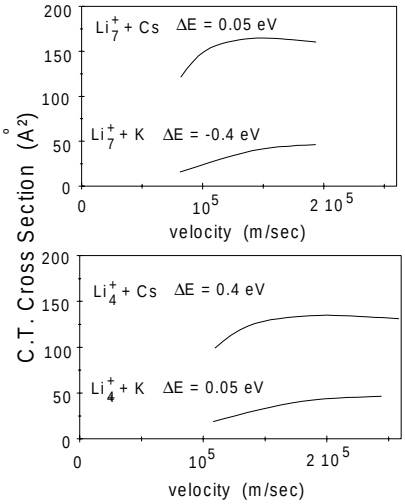

Fig. 8. Comparison of $Li_n^+ + A$ charge transfer velocity profiles for charge transfer collision of a given cluster ion with two different targets.

Charge transfer is observed with comparable efficiencies for exothermic (n = 4, 6, 8), quasi-resonant (n = 5, 7, 10) or endothermic reactions. Coupling between external and internal degrees of freedom may occurs, and C.T. toward an excited state of the projectile cannot be excluded. In that case, the electronic excitation relaxes at a time scale $< 10^{-12}$ s into vibrational excitation, followed by evaporative cooling. An atom evaporation from a neutral cluster can be experimentally characterized by the corresponding kinetic energy release, observable through a time-of-flight mass spectrum peak broadening. In order to estimate the energy transfer which may occur during the charge transfer, we measure the time-of-flight width of the neutral products mass peak. The sensitivity of our measurement allows us to exclude the deposition of more than 0.3 eV into the cluster. This excludes a charge transfer toward an excited state lying more than 0.3 eV above the cluster ground state.

It is well-known that the amplitude of the charge transfer cross-section depends on collision energy defect but also the electronic clouds of the collisional partners, as interpreted for example by Rapp and Francis [25]. Comparison of the results obtained when changing the target demonstrate the importance of the second point. Figure 8 shows that C.T. is more efficient for $Li_7^+ + Cs$, nearly resonant with $\Delta E = 0.05$ eV, than for $Li_7^+ + K$, less resonant with $\Delta E = -0.4$ eV. But Figure 8 also indicates that $Li_4^+ + K$, nearly resonant with $\Delta E = 0.05$ eV, provides a cross-section much lower than $Li_4^+ + Cs$, less resonant with $\Delta E = 0.42$ eV. More generally, C.T. is more efficient for Li_n^+ collisions with cesium than with potassium atoms (Fig. 6), even when the energy defect is lower in the first case. This sustains that the role of the target can be of importance.

Geometrical size of the partners may also influence C.T. efficiency. Hard sphere collisional cross-sections can be defined by $\sigma_{\text{hs}} = \pi(r_{\text{s}} n^{1/3} + r_A)^2$ where the Wigner-Seitz radius r_{s} characterizes the electronic density within

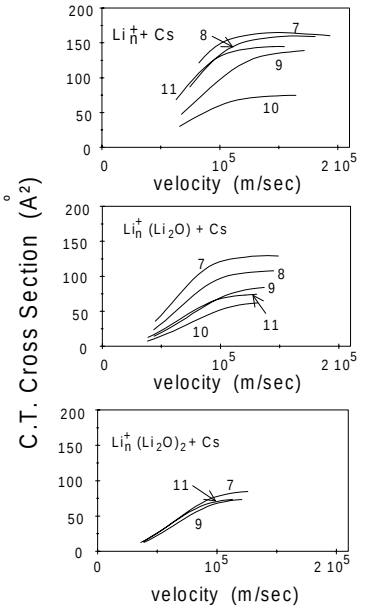

Fig. 9. Size effects in the variation of absolute charge transfer cross-section profiles for $Li_n^+ + Cs$ (upper part), $Li_n^+(Li_2O) + Cs$ (middle part) or $Li_n^+(Li_{2O})_2 + Cs$ collisions ($n = 7-11$).

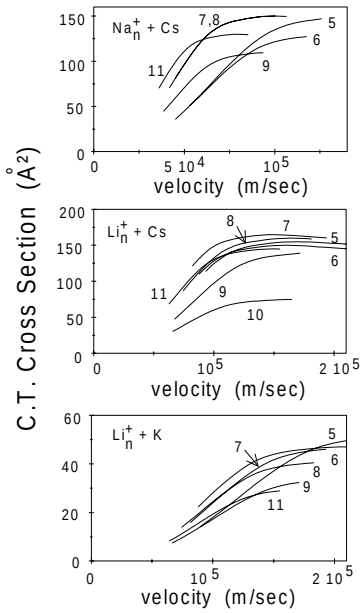

Fig. 10. C.T. velocity profile for various $M_n^+ + A$ system, illustrating similarities in the relative position of the curves for n in the range $n = 5$ to 11. The C.T. velocity profiles have not been measured for $Na_{10}^+ + Cs$ or $Li_{10}^+ + K$ systems because of the very low neutral product signal.

the bulk. r_A is the target atomic radius. Obviously, the measured σ_m parameters are smaller and for large sizes much smaller than the hard-sphere cross-sections. This means that the electron transfer probability is much smaller than unity along the trajectory.

However, charge transfer is efficient when there is a good overlap of the collision partner electronic clouds. This overlap is achieved for a larger internuclear distance in the case of collisions with a cesium atom, because the hydrogenoid orbitals are more extended for Cs than for K, and also because Cs has a larger polarizability (59.6 Å^3) than K (43.4 Å^3) [31], allowing a larger deformation of the Cs electronic cloud on the internuclear axis and a better overlap.

Charge transfer patterns between the target and a metal cluster M_n^+ evolve in a non monotonic way for small particles, but reach in the 15–25 size range characteristics evoking charge transfer between the target and the bulk M surface. In this frame, C.T. between a given M_n^+ cluster and A is strongly marked by the target A characteristics. The charge transfer between a particle and a metal surface is discussed in terms of work function and energy defect. It also depends on the metal electronic properties, interpreted in term of electron screening and level density. Our data tend to prove that the second point remains pertinent even in very small metallic particles.

3.3 Charge transfer cross-section profile and projectile size effects

We focus now on the evolution of C.T. velocity profiles when changing the size and the nature of the cluster, for a given target.

A striking point appears in the evolution of C.T. profiles when varying cluster size in the range $n = 7...11$ for the collision $Li_n^+ + Cs$. As observed in Figure 9, there is an abrupt drop in the C.T. efficiency for $n = 10$. Such an effect is also observed, to a less extent, for $n = 22$ (Fig. 6).

We checked that this point can be related to an electronic property by shifting the number of atoms in the projectile while keeping the same number of delocalized electrons: we measured C.T. cross-sections for $Li_n^+(Li_2O)_p$ clusters ($p = 1...4$). In a previous experiment [33], we have shown that these systems exhibit the same shell effects in the mass spectra intensities as Li_n^+. Consequently, they contain the same number n of delocalized electrons in the metallic part of the particle. As observed in Figure 9, C.T. cross-sections present the same patterns for Li_n^+, $Li_n^+(Li_2O)$ and $Li_n^+(Li_2O)_2$ (with less contrast as p increases), showing that the relative C.T. efficiency depends on the number of delocalized electrons, rather than on the number of lithium atoms in the particle. If we note $n_{\mathrm{cl.}}$ the number of delocalized electrons providing an electronic shell closure in the cluster ion, the cross-sections present a minimum for $n = n_{\mathrm{cl.}} + 1$, in the three above mentioned cases. This effect cannot be explained by the local variations of ionization energies or polarizabilities [34,35] with cluster size and underlines the importance of the quantum size electronic effects.

C.T. velocity profiles present similarities when changing either the projectile or the target. Figure 10 presents the profiles measured for different cluster sizes for $Na_n^+ +$ Cs, $Li_n^+ + Cs$ and $Li_n^+ + K$ systems. The relative positions of the curves on each graph are approximately the same for the three systems and also for $Li_n^+(Li_2O) + Cs$ collisions

(Fig. 9). The jellium description of metal-atom clusters [2] predicts that the electronic structure and the geometrical shape are governed by the number of delocalized electrons, showing marked quantum size effects independent of the cluster metallic part constituent provided that the metallic nature of the bonding is preserved. The qualitatively similar evolution with n of C.T. cross-sections for various $M_n^+ + A$ systems demonstrates again the role of quantum size effects in the electron transfer involving small metallic clusters.

Comparing now collisions involving lithium and sodium clusters it appears that in the mass range $n = 15-50$, σ_m is approximately constant for lithium clusters whereas it decreases for sodium particles. This might be partly explained by the following process [15]. Once an electron has been transferred from the target to the cluster, the valence electrons of the aggregate are attracted by the target ion, because of the large polarizability of the metal particle [34,35]. The probability that one of the n delocalized electrons jumps back to the target increases with increasing n. The net result is a decrease of the C.T. cross-section. This effect is expected to be stronger for sodium particles nearly twice as polarizable as lithium clusters at a given number of atoms. Lithium or sodium clusters are expected to be metallic particles even for a small number of atoms, but we observe here a property illustrating a significant difference in their electronic properties. Charge transfer is a local probe of the electronic properties of a metallic system. Differences between C.T. efficiencies for Na_n^+ and Li_n^+ clusters colliding with cesium atoms may originate from the screening effects used to interpret the differences in the corresponding bulk properties. Such a screening effect has already been invoked to explain the differences observed in Na_n^+ and Li_n^+ electronic responses to photoexcitation [36].

4 Conclusion

We have presented a systematic study of absolute integral cross-sections for collisions between free lithium (sodium) cluster ions as projectiles and cesium (potassium) atoms as targets. The main results can be summarized as follows.

For a collision energy within 1–10 keV in the laboratory frame, the electron transfer is efficient for cluster ionization potentials within a few tenth of eV around the atom target ionization potential. The velocity profiles present the typical patterns of non resonant atom-atom collisions with a velocity threshold in the range of 5×10^4 m/s and a maximum in the range of 10^5 m/s.

The evolution of C.T. efficiency when changing the target qualitatively obey the Massey criterion for large clusters. But the interpretation of the $M_n^+ + A$ data in term of collision energy defect is not so simple for small clusters. A key point is to know whether cluster excited electronic states play a significant role in the collisional process.

The velocity providing the most efficient charge transfer is smaller than the typical value for the $M^+ + A$ ion-atom collision, decreases with increasing cluster size and merge the range of the typical velocity for an efficient atom-metal surface charge transfer. The $M_n^+ + A$ collision resembles the atom-metal surface situation for $n > 15-20$ typically.

Shell effects are observed with a minimum C.T. efficiency for projectile ions containing 9 and 21 delocalized electrons. Similarities observed in the velocity profiles for charge transfer to small metallic cluster ions, when changing either the projectile or the target, illustrate the importance of the cluster electronic structure in the C.T. process. There is need for further investigation of the role of cluster shell structure in collisions.

Differences are observed in the evolution of cross-sections with cluster size for electron transfer to lithium and to sodium cluster ions ($n = 15...50$). This raises the question of the limits of metallicity in very small particles.

References

1. W.A. de Herr, Rev. Mod. Phys. **65**, 611 (1993).
2. M. Brack, Rev. Mod. Phys. **65**, 677 (1993).
3. R. Schlipper, R. Kusche, B. von Issendorff, H. Haberland, Phys. Rev. Lett. **80**, 1194 (1998).
4. C.A. Ullrich, P.G. Reinhard, E. Suraud, J. Phys. B: At. Mol. Opt. Phys. **30**, 5043 (1997).
5. C. Bréchignac, Ph. Cahuzac, J. Leygnier, R. Pflaum, J. Weiner, Phys. Rev. Lett. **61**, 314 (1988).
6. F. Chandezon, C. Guet, B.A. Huber, D. Jalabert, M. Maurel, E. Mommand, C. Ristori, J.C. Rocco, Phys. Rev. Lett. **74**, 3784 (1995).
7. P.G. Reinhard, E. Suraud, C.A. Ullrich, Eur. Phys. J. D **1**, 303 (1998).
8. M.F. Politis, P.A. Hervieux, J. Hanssen, M.E. Madjet, F. Martin, Phys. Rev. A **58**, 367 (1998).
9. O. Knospe, L. Jellinek, U. Saalmann, R. Schmidt, Eur. Phys. J. D **5**, 1 (1999).
10. W.A. Saunders, Phys. Rev. Lett. **62**, 1037 (1989).
11. N.D. Bhaskar, R.P. Frueholz, C.M. Klimcak, R.A. Cook, Chem. Phys. Lett. **154**, 175 (1989).
12. M. Abshagen, J. Kowalski, M. Meyberg, G. zu Putlitz, F. Träger, J. Well, Europhys. Lett. **5**, 13 (1988).
13. M. Abshagen, J. Kowalski, M. Meyberg, G. zu Putlitz, J. Slaby, F. Träger, Chem. Phys. Lett. **174**, 455 (1990).
14. S.B.H. Bach, J.R. Eyler, J. Chem. Phys. **92**, 358 (1990).
15. C. Bréchignac, Ph. Cahuzac, F. Carlier, J. Leygnier, I.V. Hertel, Z. Phys. D **17**, 61 (1990).
16. M. Bacal, W. Reichelt, Rev. Sci. Instrum. **45**, 769 (1974).
17. W.C. Wiley, I.H. Mc Laren, Rev. Sci. Instrum. **26**, 1150 (1955).
18. C. Bréchignac, Ph. Cahuzac, J.Ph. Roux, D. Pavolini, F. Spiegelmann, J. Chem. Phys. **87**, 5694 (1987).
19. C.E. Klots, Z. Phys. D. **5**, 83 (1987).
20. C. Bréchignac, H. Busch, Ph. Cahuzac, J. Leygnier, J. Chem. Phys. **101**, 6992 (1994).
21. A.S. Tremsin, J.F. Pearson, J.E. Lees, G.W. Fraser, Nucl. Instrum. Meth. Phys. Res. A **386**, 719 (1996).
22. C. Bréchignac, Ph. Cahuzac, J. Leygnier, J. Weiner, J. Chem. Phys. **90**, 1492 (1989).
23. E.W. Kaiser, A. Crowe, W.E. Falconer, J. Chem. Phys. **61**, 2720 (1973).

24. J. Perel, H.L. Daley, *Electronic and atomic collisions*, abstract of papers VIII ICPEAC, Vol. II, edited by B.C. Cobic, M.V. Kurepa (Beograd, Yougoslavia, 1973).
25. D. Rapp, W.E. Francis, J. Chem. Phys. **37**, 2361 (1962).
26. R.E. Olson, Phys. Rev. A **6**, 1822 (1972).
27. We also used a Landau-Zener profile, from R.J. Fortner, B.P. Curry, R.C. Der, T.M. Kavanagh, J.M. Khan, Phys. Rev. **185**, 164 (1969), and got the same v_m and σ_m fitting parameters.
28. H.S.W. Massey, Rept. Progr. Phys. **12**, 248 (1949).
29. J. Perel, H.L. Daley, Phys. Rev. A **4**, 162 (1971).
30. Ph. Dugourd, D. Rayane, P. Labastie, B. Vezin, J. Chevaleyre, M. Broyer, Chem. Phys. Lett. **197**, 433 (1992).
31. *C.R.C. Handbook of Chemistry and Physics 74th*, edited by D.R. Lide (C.R.C Press Inc., 1993).
32. J. Los, J.J.C. Geerlings, Phys. Rep. **190**, 133 (1990).
33. C. Bréchignac, Ph. Cahuzac, M. de Frutos, P. Garnier, Z. Phys. D **42**, 303 (1997).
34. W.D. Knight, K. Clemenger, W.A. de Heer, W.A. Saunders, Phys. Rev. B **31**, 2539 (1985).
35. E. Benichou, R. Antoine, D. Rayane, B. Vezin, F.W. Dalby, Ph. Dugourd, M. Broyer, C. Ristori, F. Chandezon, B.A. Huber, J.C. Rocco, S.A. Blundell, C. Guet, Phys. Rev. A **59**, R1 (1999).
36. C. Bréchignac, Ph. Cahuzac, J. Leygnier, A. Sarfati, Phys. Rev. Lett. **70**, 2036 (1993).